COMMUNICATIONS IN COMPUTATIONAL PHYSICS
Vol. **6**, No. 2, pp. 354-366

Commun. Comput. Phys.
August 2009

# Numerical Study on the Tortuosity of Porous Media via Lattice Boltzmann Method

Jianhua Lu[1], Zhaoli Guo[1], Zhenhua Chai[1] and Baochang Shi[2,*]

[1] *State Key Laboratory of Coal Combustion, Huazhong University of Science and Technology, Wuhan, 430074, China.*
[2] *School of Mathematics and Statistics, Huazhong University of Science and Technology, Wuhan, 430074, China.*

Received 11 April 2008; Accepted (in revised version) 23 October 2008

Communicated by Sauro Succi

Available online 15 December 2008

**Abstract.** In this paper, we simulate the pressure driven fluid flow at the pore scale level through 2-D porous media,which is composed of different curved channels via the lattice Boltzmann method. With this direct simulation, the relation between the tortuosity and the permeability is examined. The numerical results are in good agreement with the existing theory.

**AMS subject classifications**: 76S05, 80M25

**Key words**: Tortuosity, lattice Boltzmann, porous media, pore scale.

## 1 Introduction

Fluid flow through porous media is a common phenomenon in science and engineering. Thus, the prediction of the permeability, as the main transport property in porous media, is a long-standing problem of great practical importance. Existing experiment results and theoretical works [1–5] show that the permeability of various porous materials is determined by their structure parameters such as porosity, specific surface area, tortuosity etc. Among the existing theories, the Kozeny-Carman equation may be the most famous one, which can be expressed as:

$$k=\frac{\epsilon^3}{k_0 T^2 S^2}, \tag{1.1}$$

*Corresponding author. *Email addresses:* plough0@gmail.com (J. Lu), zlguo@hust.edu.cn (Z. Guo), hustczh@126.com (Z. Chai), sbchust@126.com (B. Shi)

 

where $k$ is the permeability, $k_0$ is the shape factor, $\epsilon$ is the porosity and $S$ is the specific surface area (i.e., the pore surface area per unit volume of porous material) and $T$ is the tortuosity, defined as follows:

$$T = \frac{L_e}{L}, \tag{1.2}$$

where $L_e$ is the length of real flow path and $L$ is the length of sample of the porous material. According to Eq. (1.1), the square of tortuosity is inversely proportional to the permeability if $\epsilon^3/k_0S^2$ is fixed. However, this relation is always assumed to be applicable for various porous materials although it is only analytically derived from rather simple inclined straight channel model [15–17]. To our knowledge, few works is available to test this relation in more complex cases via experiments or numerical simulations.

In recent decades, with the development of computer and numerical algorithms, numerical studies for fluid flow in porous media with extremely complex structures is possible. The lattice Boltzmann (LB) method, which appeared recently for simulating fluid flow has widely used in understanding the transport process in porous media at the pore scale level [6–8,11,12,15,18–26] due to its advantages such as easily dealing with complex boundaries over other simulation methods as finite volume method. However, few literature is available to study the relation between the tortuosity and the permeability using LB methods yet. In this work, we will focus on this topic by simulating the fluid flow at the pore scale level in some 2D porous media composed of different curved capillary channels via the lattice Boltzmann method.

Our paper is organized as follows: in Section 2 three test cases for 2D porous media are presented in order to test the relation between the permeability and the tortuosity; in Section 3 the LB model used in this paper is briefly introduced; in Section 4 the relation between the tortuosity and the permeability is examined and the numerical results obtained are compared with the Kozeny-Carman equation. Finally in Section 5 some conclusions are presented.

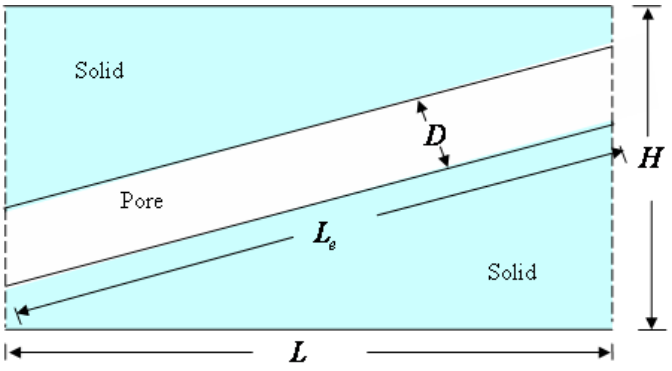


Figure 1: The Layout of a capillary model with inclined straight channel, i.e., Case I.

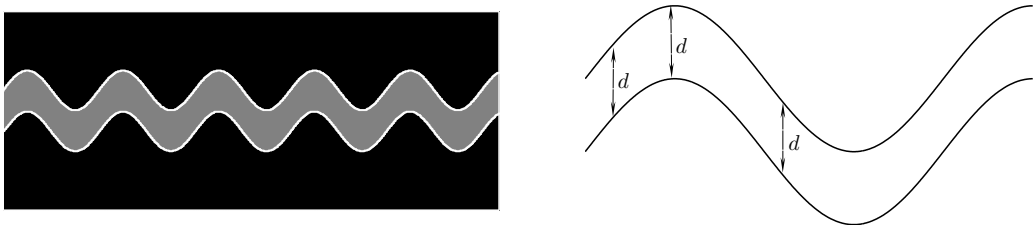


(a) (b)

Figure 2: (a) The layout of a capillary model with a curved channel whose boundary sin-type, i.e., Case II. (b) A simple section.

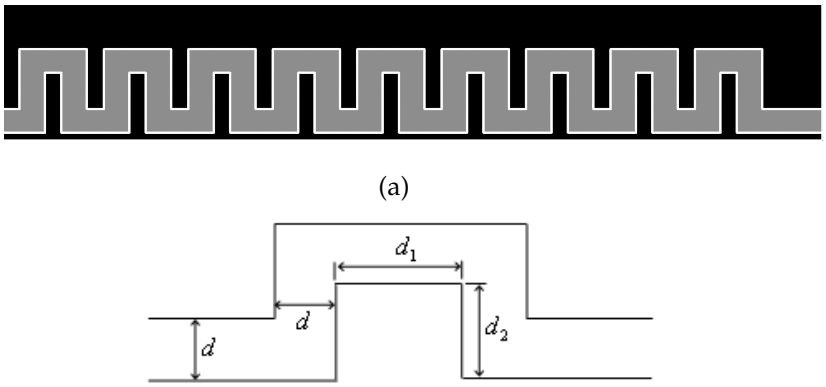


(a)

(b)

Figure 3: (a)The layout of a capillary model with a curved channel whose boundary zigzag-type, i.e., Case III. (b) A sample section.

## 2 Test cases

For the purpose of studying the relation between the tortuosity and the permeability, three test cases corresponding different capillary models for 2D porous media are examined. Case I, as shown in Fig. 1, is a capillary model with inclined straight channel. Case II (Fig. 2) and Case III (Fig. 3) are capillary models with curved channels whose boundary are sin-type and serpentine respectively. In all these test cases, we assume that the Darcy's law, namely,

$$\bar{u} = -\frac{k}{\nu}\nabla p \tag{2.1}$$

is valid, where $\bar{u}$ is the average velocity of the whole sample along the direction of the pressure gradient, $\nabla p$ is the pressure gradient added at the left and right boundary of the sample, $\nu$ is the kinematic viscosity. For Case I, an analytical solution for the permeability

can be found as [15]:

$$k=\frac{\epsilon^3}{3T^2S^2}, \tag{2.2}$$

where $\epsilon=DT/H$, $S=2T/H$, and $D$ is the width of the channel. On the other hand, we can measure the permeability according to Eq. (2.1) from the numerical results:

$$k=-\frac{\nu\bar{u}}{\nabla p}. \tag{2.3}$$

If the pressure on the left boundary is denoted as $p_{in}$ and the one on the right boundary as $p_{out}$, Eq. (2.3) can be rewritten as

$$k=\frac{\nu\bar{u}L}{p_{in}-p_{out}}. \tag{2.4}$$

So for this case, we can compare the numerical solutions with the analytical ones. However, we have no analytical solutions for Case II and Case III. In addition, it is not easy to determine the shape factor $k_0$ in these two cases. Therefore, it is difficult to examine the relation between the permeability and the tortuosity directly. In this work, instead of directly examining this relation, we examine that between $-\nu S^2\bar{u}/\epsilon^3\nabla p$ and $1/T^2$. To this end, from Eq. (1.1) with Eq. (2.1), we can get:

$$-\frac{\nu S^2\bar{u}}{\epsilon^3\nabla p}=\frac{1}{k_0T^2}, \tag{2.5}$$

or

$$\frac{\nu S^2\bar{u}L}{\epsilon^3(p_{in}-p_{out})}=\frac{1}{k_0T^2}, \tag{2.6}$$

where $L$ is the length of the porous sample. So we can test if $-\nu S^2\bar{u}/\epsilon^3\nabla p$ is proportional to $1/T^2$ instead of examine the relation between the permeability and the tortuosity in these two cases.

## 3 The LB method

The lattice Boltzmann method has been proved to be a very efficient simulation tool to study fluid flows in highly complex geometries such as porous media. In this work, we will use the impressible LB model proposed by Guo in [28] (D2G9), which was developed from the classical models in [6, 9, 10]. In this model, the lattice Boltzmann equation with the BGK approximation can written as

$$g_i(\boldsymbol{x}+\boldsymbol{c}_i\delta t,t+\delta t)-g_i(\boldsymbol{x},t)=-\frac{1}{\tau}(g_i(\boldsymbol{x},t)-g_i^{eq}(\boldsymbol{x},t)), \tag{3.1}$$

where $g_i$ is the single particle mass distribution function in $i$ direction, $\delta t$ and $c_i\delta t$ are the time and space increment, respectively; $\tau$ is the relaxation time due to collision. The discrete velocities $c_i$'s are defined as

$$\boldsymbol{c}_i=\begin{cases}(0,0), & i=0,\\ (\cos[(i-1)\pi/2],\sin[(i-1)\pi/2])c, & i=1,2,3,4,\\ (\cos[(2i-9)\pi/4],\sin[(2i-9)\pi/4])\sqrt{2}c, & i=5,6,7,8,\end{cases}$$

where the velocity $c$ is $\delta x/\delta t$. Moreover, $g_i^{eq}$ is the local distribution function given by

$$g_i^{eq}=\begin{cases}\rho_0-\frac{5p}{3c^2}+s_0(\boldsymbol{u}), & i=0,\\ \frac{p}{3c^2}s_i(\boldsymbol{u}), & i=1,2,3,4,\\ \frac{p}{12c^2}s_i(\boldsymbol{u}), & i=5,6,7,8,\end{cases}$$

where

$$s_i(\boldsymbol{u})=-\omega_i\Big[\frac{\boldsymbol{c}_i\cdot\boldsymbol{u}}{c_s^2}+\frac{(\boldsymbol{c}_i\cdot\boldsymbol{u})^2}{2c_s^4}-\frac{|\boldsymbol{u}|^2}{2c_s^2}\Big] \tag{3.2}$$

with the weight coefficient

$$\omega_i=\begin{cases}4/9, & i=0,\\ 1/9, & i=1-4,\\ 1/36, & i=5-8,\end{cases}$$

and $c_s=c/\sqrt{3}$.

From Eq. (3.1), we can obtain the incompressible Navier-Stokes equations by using the Chapman-Enskog expansion under the assumption of the low Mach number:

$$\nabla\cdot\boldsymbol{u}=0,$$
$$\frac{\partial\boldsymbol{u}}{\partial t}+\boldsymbol{u}\cdot\nabla\boldsymbol{u}=-\nabla p+\nu\nabla^2\boldsymbol{u},$$

where the kinematic viscosity is defined as $\nu=(\tau-1/2)c^2\delta t/3$. Since the curved boundaries must be considered in the present work, we validate the code of this model by simulating a 2-D Poiseuille flow in a plane channel, where the two walls are not placed on the computation grids (see Fig. 4). The analytical solution of the steady Poiseuille flow is

$$u(x,y,t)=\frac{(p_{in}-p_{out})H^2}{4\nu}\Big[\frac{y}{H}-(\frac{y}{H})^2\Big], \tag{3.3a}$$
$$v(x,y,t)=0, \tag{3.3b}$$
$$p(x,y,t)=p_{in}-\frac{p_{in}-p_{out}}{L}x, \tag{3.3c}$$

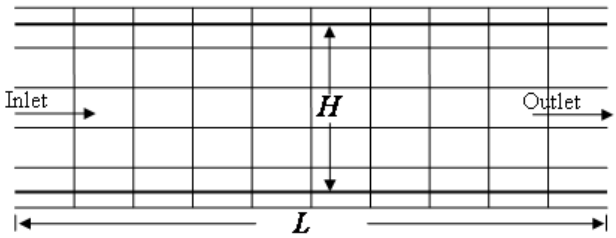


Figure 4: The layout of a 2-D Poiseuille flows, where $H$ and $L$ are the width and the length of the channel, respectively.

where $\nu$ is the kinematic viscosity of the fluid, $p_{in}$ is the pressures at the inlet and $p_{out}$ is outlet of the channel respectively. In simulation, we set $\nu=0.01$, $p_{in}=1.001$, $p_{out}=1.000$, $L=2.0$, $H=0.97$. The initial and boundary conditions here are set as

$$\begin{aligned}&u(x,y,0)=0,\quad v(x,y,0)=0,\quad p(x,y,0)=p_0,\\&p(0,y,t)=p_{in},\quad p(L,y,t)=p_{out},\\&u(x,0,t)=u(x,H,t)=0,\quad v(x,0,t)=v(x,H,t)=0.\end{aligned}$$

The lattice size in computation is $200\times100$, and the relaxation time $\tau$ is taken as 1.0. None of the wall boundaries lay on the computational grid points. The half bounce-back method [29] is used to deal with the wall boundaries (i.e., the up and down boundaries), and the non-equilibrium extrapolation method [30] is applied to the inlet and outlet boundaries. It is observed that the numerical results agree well with the analytical solution given by Eq. (3.3).

## 4 Numerical results and discussions

In this section, fluid flow through three models of porous media presented in Section 2 is simulated via the lattice Boltzmann method introduced in Section 3. We discuss the results one by one. It should be pointed out that the values of the parameters used in all our simulations, such as $\nabla p=(p_{in}-p_{out})/L$, are chosen to keep Darcy's law (2.1) valid. As we know, Darcy's law is valid when the pore scale Re is small enough. If we fix the kinematic viscosity and the pore size, the condition means that $\nabla p$ should be small enough. In Case I, for example, when $\nu=0.01$, $L=H=1.000$ and $D=0.25$, Re is less than 1.0 and the maximum relative errors defined as

$$\text{MRER}=\max\frac{|k_{as}(T)-k_{ns}(T)|}{k_{as}(T)} \tag{4.1}$$

make no obvious difference if $\nabla p<0.2$. Here $as$, $ns$ in (4.1) mean the analytical and numerical solutions, respectively. The detailed result is shown in Fig. 5. Thus we choose $\nabla p=0.001$ in Case I for simplicity.

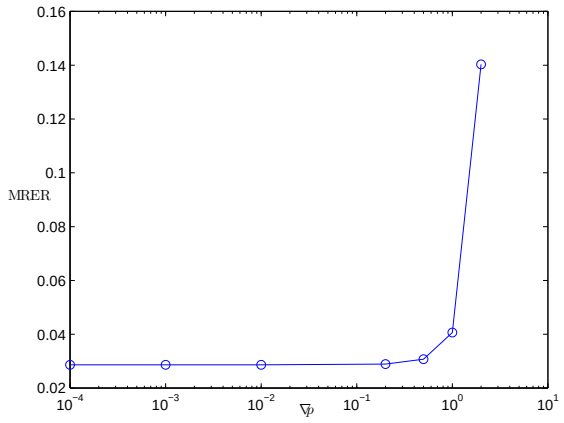


Figure 5: The maximum relative error defined by (4.1) vs $\nabla p$, where $\nu = 0.01$, $L = H = 1.0$, $D = 0.25$. The relaxation time $\tau = 1.0$, and the lattice size takes as $500 \times 500$.

### 4.1 Test case I

As mentioned in Section 2, this case is one of few cases which have the analytical solutions. In this case, we will compare the analytical solution given by Eq. (2.2) with the numerical solution of Eq. (2.3) directly. Here the inclined boundaries of the channel are given:

$$y = y_0 + ax, \quad \text{and} \quad y = y_0 + ax + D\sqrt{1+a^2}.$$

In our simulations, the lattice size is $500 \times 500$, $\tau$=1.0. $\nu = 0.01$, $p_{in} = 1.001$, $p_{out} = 1.000$, $L = H = 1.000$, $y_0 = 0.002$. The halfway bounce-back method is used to deal with the up and down curve boundaries and the non-equilibrium extrapolation method is used to deal with the inlet and outlet ones. It should be noted that the same methods are applied in the numerical simulations on Test Cases II and III. In order to examine the relation between the tortuosity and the permeability, we fix $D$ and change $a$ to get different tortuosity values and then calculate the corresponding values of the permeability from Eqs. (2.2) and (2.3) respectively. The numerical experiments are performed for four cases $D$=0.1,0.15,0.2,0.25. The comparison of the numerical and analytical solutions are shown in Figs. 6 and 7. As seen from these two figures, the numerical solutions agree well with the analytical ones for all cases. However, the deviation is also obvious. Through detailed investigations, we find that the following three main reasons lead to the errors: the lattice size, the selection of $y_0$ and the edge effect. As can be observed in Fig. 6(a) (for $D = 0.10$) and Fig. 6(b) (for $D = 0.15$), the maximum deviation from the analytical solution to the numerical solution shifts from mid $T$ to large $T$. The main reason is that the lattice size is not fine enough. If the lattice size is $1000 \times 1000$, the abnormal phenomena will disappear (see Figs. 6 and 7(a)). Since the halfway bounce back method is used in dealing with the wall boundaries, the selection of $y_0$ deadly influences the accuracy of this method. However, the selection of $y_0 = 0.002$ is not the optimal one. The numerical errors will reduce if $y_0 = 0.003$, as shown in Figs. 6 and 7. Because the analytical solution is correct

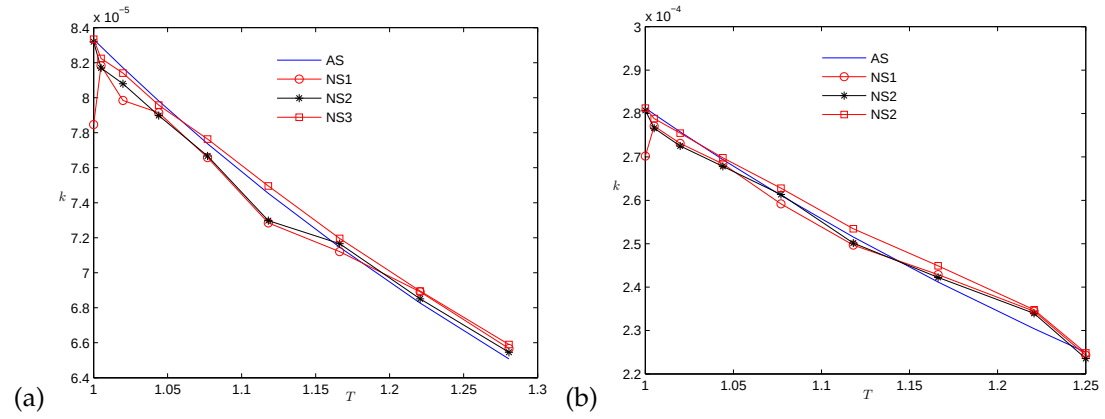


Figure 6: Comparison of the numerical solutions (NS for short) with the analytical solutions (AS for short), where $D=0.10$ for (a) and $D=0.15$ for (b). Here NS1 corresponds to $y_0=0.002$ and NS2 corresponds to $y_0=0.003$. The lattice size is $500\times500$ in both cases. NS3 corresponds to $y_0=0.0015$; and the lattice size is $1000\times1000$ in this case.

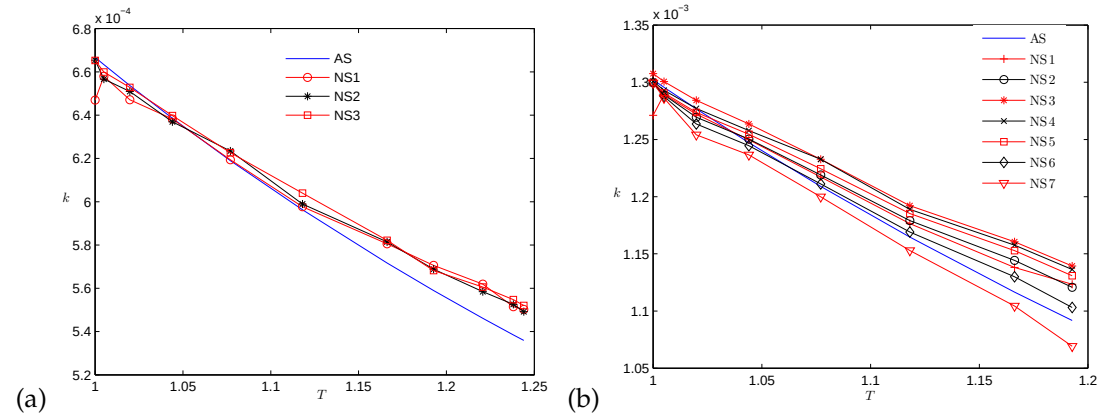


Figure 7: Comparison of the numerical solutions (NS for short) with the analytical solutions (AS for short), where $D=0.20$ for (a) and $D=0.25$ for (b). NS1 corresponds to $y_0=0.002,\tau=1.0$; NS2 corresponds to $y_0=0.003,\tau=1.0$, and NS3$\sim$7 corresponds to $y_0=0.003,\tau=4.0,2.0,1.33,0.8,0.67$ with $D=0.25$, respectively. The lattice size is $500\times500$ in all cases except NS3 for $D=0.20$ where the lattice size is $1000\times1000$ and $y_0=0.0015$.

only under the assumption that the channel is long enough, the edge effect is obvious if the assumption is not satisfied. This effect is more obvious in the case $D=0.25$ when $T$ is large. As shown in Fig. 7(b), the maximum relative error (MRER) of NS2 is 2.66% for $T=1.1927$. If we lengthen the channel by two times, the relative error then reduces to 1.11% for the same $T$ as shown in Fig. 8. In addition, the relaxation time $\tau$ should also be chosen properly because the permeability calculated by LBM (for traditional single relaxation time models) is dependent on the kinematic viscosity (through $\tau$), which was first noticed by Ferriol [13]. As shown in Fig. 7(b), the optimal value of $\tau$ should be 0.8, which is about 1.0 as recommended by Jin [14]. To balance the accuracy and the computational

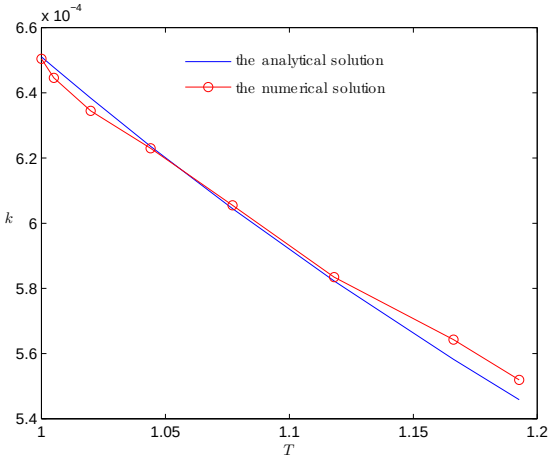


Figure 8: Comparison of the numerical solutions with the analytical solutions, where $D=0.25$. Here $H=L=2.0$, $y_0=0.0015$, $pin=1.001$, $pout=1.000$, the lattice size is $1000\times1000$ and $\tau=1.0$.

cost, we control the relative error less than 5%, although the situation is improved if we deal well with the above reasons.

## 4.2 Test case II

In this subsection, we examine the relation $-\nu S^2\bar{u}/\epsilon^3\nabla p$ and $1/T^2$ instead of that between the permeability and the tortuosity. The same procedure will apply to Case III. From Eq. (2.5), $-\nu S^2\bar{u}/\epsilon^3\nabla p$ is proportional to $1/T^2$. We will focus on the extent to which the relation is true.

Here the sine-type boundaries of the channel are given:

$$y=y_0+a\sin 2\pi\omega x, \quad y=y_1+a\sin 2\pi\omega x,$$

where $d=y_1-y_0>0$.

In the simulations, the lattice size is $512\times256$, $\tau=1.0$. $\nu=0.01$, $p_{in}=1.01$, $p_{out}=1.00$, $L=20.00$, $H=10.00$. We fix $d$ and $a$, and change the tortuosity by altering $\omega$ in our numerical experiments. Fig. 9 shows the numerical results of two cases: (a) $d=2.00$,$a=1.00$; (b) $d=3.00$,$a=2.00$. As shown in Fig. 9, $-\nu S^2\bar{u}/\epsilon^3\nabla p$ is indeed proportional to $1/T^2$ approximately, which implies clearly the validation of Kozeny-Carman formula. However, The intercepts of the fitting line are 0.017 for (a) and $-0.0098$ for (b), which seems to be in contradiction to Kozeny-Carman formula where the intercept is zero. In addition, we can also see that the absolute value of the intercept is getting larger as the ratio $d/a$ increases. Results on other cases such as $d=3.00$, $a=1.00$ also show this tendency. This kind of phenomena may be due to two reasons. First one is the numerical errors in the simulations. If the simulation performed on such as the finer lattice size, the proper selection of $y_0$ and $\omega$, the intercepts will be more closer to zero; The second one is the departure the geometry tortuosity of the channel from the tortuosity of real flow path. In all our

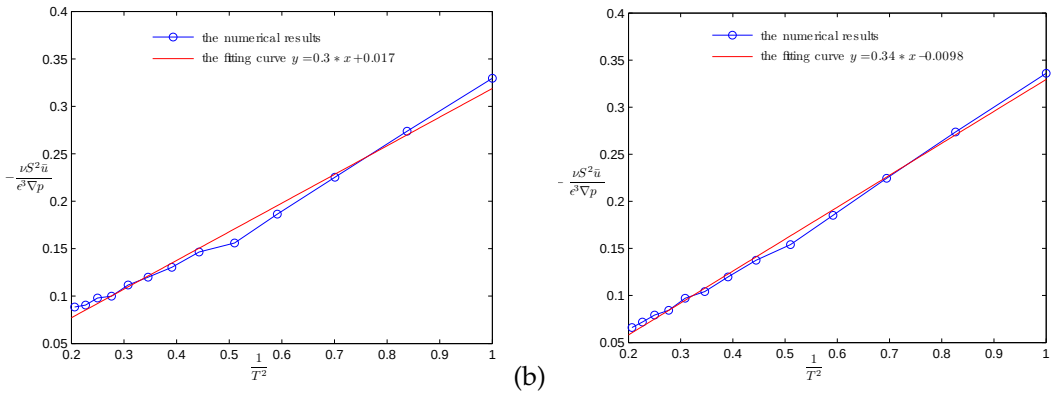


Figure 9: The relation between $-\nu S^2\bar{u}/(\epsilon^3\nabla p)$ and $1/T^2$ in Case II. Here $d=2.0$, $a=1.0$ for (a) and $d=3.0$, $a=2.0$ for (b).

simulations, we use the geometry one for convenience. This kind of phenomena shows that the tortuosity used in Kozeny-Carman (1.1) should be that of the real path flow.

### 4.3 Test case III

In simulation, the lattice size is $1000\times180$, $\tau=1.0$. $\nu=0.01$, $p_{in}=1.01$, $p_{out}=1.00$, $L=10.00$, $H=1.80$. We fix $d$ and $d_1$, and alter the tortuosity of the channel by changing $d_2$, as shown in Fig. 3(b). Here the numerical experiments are done in the following four cases $d_1=0.20,0.30,0.40,0.50$ where $d=0.30$. The numerical results are shown in Figs. 10 and 11. From these figures, we can easily find that $-\nu S^2\bar{u}/\epsilon^3\nabla p$ is proportional to $1/T^2$ approximately again in this model. However, the similar phenomena which seems to be in contradiction to Kozeny-Carman formula can also be observed from these figures as in Test Case II. Similarly, the situation will be improved if better parameters affected the accuracy of the simulation and the tortuosity of real flow path are used.

In summary, the validation of Kozeny-Carman equation (1.1) can be demonstrated from the three Test Cases in certain extent. In other words, the relation between the tortuosity and the permeability implied in this formula is also true at least in these Test Cases.

## 5 Conclusion

In this paper, the pressure driven fluid flow in 2D porous media models composed of curved channels is simulated using the LB method to examine the relation between tortuosity and permeability. As shown in Section 4, the square of the tortuosity is in inverse proportion to the permeability in all of the three Test Cases under certain conditions. These results are found in good agreement with the Kozeny-Carman theory. In addition, as shown in Case II, the Kozeny-Carman theory may prefer the tortuosity with the defi-

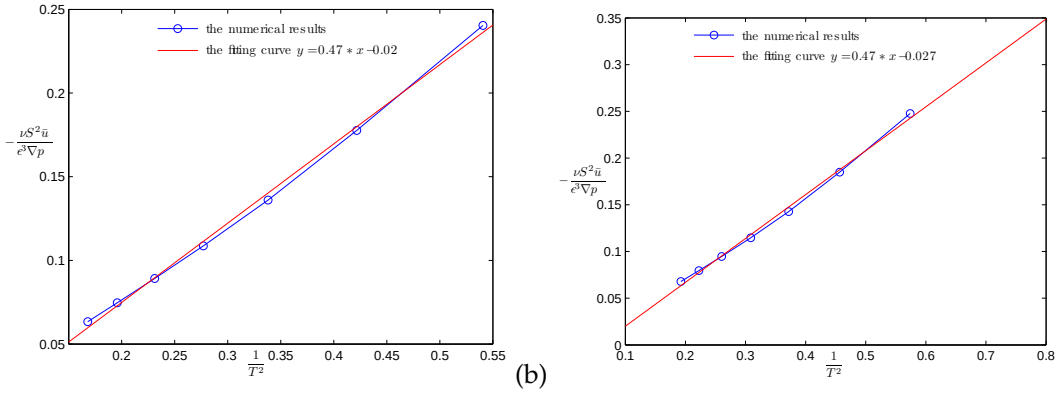


(a) (b)

Figure 10: The relation between $-\nu S^2\bar{u}/(\epsilon^3\nabla p)$ and $1/T^2$ in Case III. Here $d=0.30$, $d_2=0.20\sim0.80$. $d_1=0.20$ for (a) and $d_1=0.30$ for (b).

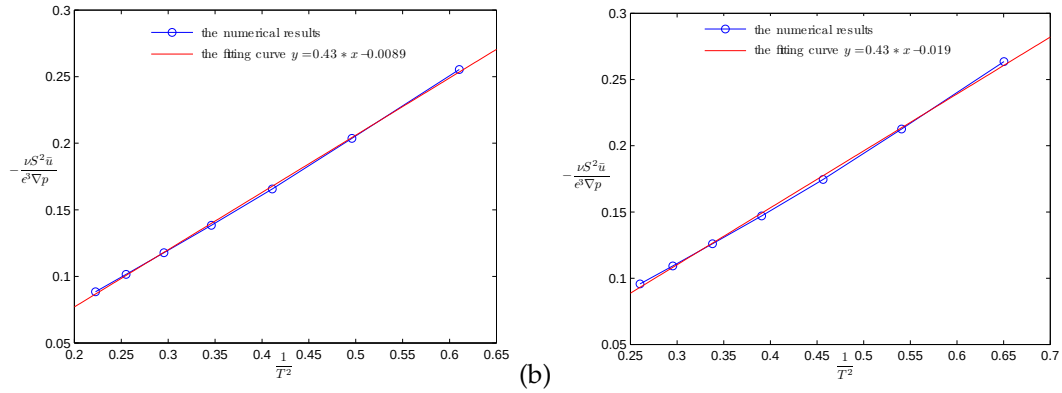


(a) (b)

Figure 11: The relation between $-\nu S^2\bar{u}/(\epsilon^3\nabla p)$ and $1/T^2$ in Case III. Here $d=0.30$, $d_2=0.20\sim0.80$. $d_1=0.40$ for (a) and $d_1=0.50$ for (b).

nition version of the real flow path. We point out that all the simulations are performed in rather simple test Cases for the 2D porous media; the situations in more complex circumstances such as 3D cases need to be further investigated.

## Acknowledgments

This work is supported by the National Basic Research Program of China (Grant No. 2006CB705804) and the National Natural Science Foundation of China (Grant No. 60773195).

### References

[1] J. Bear, Dynamics of Fluids in Porous Media, Elsevier, New York, 1972.

[2] F. A. Dullien, Porous media: Fluid Transport and Pore Structure, Academic, New York, 1979.
[3] R. E.Collins, Flow of Fluids Through Porous Materials, Reinhold, New York, 1961.
[4] A. E. Scheidegger, The Physics of Flow Through Porous Media, 3rd ed., University of Toronto, Toronto, 1974.
[5] S. Liu and J. H. Masliyah, Single fluid flow in porous media, Chem. Eng. Comm., 148-150 (1996), 653-732.
[6] Y. Qian, D. Humieres and P. Lallemand, Lattice BGK models for Navier-Stokes equation, Europhys. Lett., 17 (1992), 479-484.
[7] S. Succi, The Lattice Boltzmann Equation for Fluid Dynamics and Beyond, Oxford University, London, 2001.
[8] R. Benzi, S. Succi and M. Vergassola, The lattice Boltzmann equation: Theory and applications, Phys. Rep., 222 (1992), 145-197.
[9] S. Hou, Q. Zou, S. Chen, G. Doolen and A. C. Cogley, Simulation of cavity flow by the lattice Boltzmann method, J. Comput. Phys., 118 (1995), 329-347.
[10] X. He and L. Luo, Lattice Boltzmann methods for simulating incompressible fluid flows, Int. J. Stat. Phys., 88 (1997), 927-944.
[11] S. Succi, E. Foti and F. Higuera, Three-dimensional flows in complex geometries with the lattice Boltzmann method, Europhys. Lett., 10 (1989), 433-438.
[12] A. Cancelliere, C. Chang, E. Foti, D. H. Rothman and S. Succi, The permeability of a random medium: Comparison of simulation with theory, Phys. Fluids A, 2 (1990), 2085-2088.
[13] B. Ferreol and D. H. Rothman, Lattice-Boltzmann simulations of flow through fontainebleau sandstone, Trans. Porous Media, 20 (1995), 3-20.
[14] G. Jin, T. W. Patzek and D. B. Silin, Direct prediction of absolute permeability of unconsolidated and consolidated reservoir rock, Paper SPE 90084, in: SPE Annual Technical Conference, 2004.
[15] H. Fang, Z. Wang, Z. Liu and M. Liu, Lattice Boltzmann method for simulating the viscous flow in large distensible blood vessels, Phys. Rev. E, 65 (2002), 051925.
[16] F. Jiang, M. S. A. Oliveira and A. C. M. Sousa, Mesoscale SPH modeling of fluid flow in isotropic porous media, Comput. Phys. Comm., 176 (2007), 471-480.
[17] A. Koponen, M. Kataja and J. Timonen, Tortuous flow in porous media, Phys. Rev. E, 54 (1996), 405-409.
[18] A. Koponen, M. Kataja and J. Timonen, Permeability and effective porosity of porous media, Phys. Rev. E, 56 (1997), 3319-3325.
[19] M. L. Stewart, A. L. Ward and D. R. Rector, A study of pore geometry effects on anisotropy in hydraulic permeability using the lattice-Boltzmann method, Adv. Water Res., 29 (2006), 1328-1340.
[20] J. R. Quispea and P. G. Toledo, Lattice Boltzmann simulation of flow through two-dimensional particle sediments, Int. J. Miner. Process., 73 (2004), 91-102.
[21] M. Madadi and M. Sahimi, Lattice Boltzmann simulation of fluid flow in fracture networks with rough, self-affine surfaces, Phys. Rev. E., 67 (2003), 026309.
[22] Y. Liu, F. Zhou and G. Yan, Lattice Boltzmann simulations of the Klinkenberg effect in porous media, Chinese J. Comput. Phys., 20 (2003), 158-161.
[23] C. Pan, L. Luo and C. T. Miller, An evaluation of lattice Boltzmann schemes for porous medium flow simulation, Comput. Fluids, 35 (2006), 898-909.
[24] J. R. Quispe, R. E. Rozas and P. G. Toledo, Permeability-porosity relation from a geometrical model of shrinking and lattice Boltzmann and Monte Carlo simulations of flow in two-dimensional pore networks, Chem. Eng. J., 111 (2005), 225-236.

[25] N. Jeong, D. H. Choi and C. L. Lin, Predication of Darcy-Forchheimer drag for micro-porous structures of complex geometry using the lattice Boltzmann method, J. Micromech. Microeng., 16 (2006), 2240-2250.
[26] S. P. Sullivan, L. F. Gladden and M. L. Johns, Simulation of power-law fluid flow through porous media using lattice Boltzmann techniques, J. Non-Newtonian Fluid Mech., 133 (2006), 91-98.
[27] J. Bernsdorf, G. Brenner and F. Durst, Numerical analysis of pressure drop in porous media flow with lattice Boltzmann (BGK) automata, Comput. Phys. Comm., 129 (2000), 247-255.
[28] Z. Guo, B. Shi and N. Wang, Lattice BGK model for incompressible Navier-Stokes equation, J. Comput. Phys., 165 (2000), 298-306.
[29] D. Ziegler, Boundary conditions for the lattice Boltzmann simulations, J. Stat. Phys., 71 (1993), 1171-1177.
[30] Z. Guo, C. Zheng and B. Shi, Non-equilibrium extrapolation method for velocity and pressure boundary conditions in the lattice Boltzmann method, Chinese Phys., 11 (2002), 366-374.